Title: Neoadjuvant Botensilimab/Balstilimab for localized mismatch repair proficient and deficient colon cancer: Results of the NEST phase 2 clinical trial

Running title (54/60 char): Neoadjuvant botensilimab/balstilimab in colon cancer

Authors: Manish A. Shah[1*], Erika Hissong[2], Mehraneh D Jafari[3], Pashtoon Murtaza Kasi[1], Maider Astorkia[4], Sahrish Khan[1], Casey Owens[1], Zhengming Chen[5], Heather Yeo[3], Fabio Socciarelli[2], Sandipto Sarkar[1], Alana Nguyen[1], Despina Siolas[1], Allyson Ocean[1], Kelly Garrett[3], Lea Lowenfeld[3], Alessio Pigazzi[3], Preethi Guniganti[6], Sanjay Patel[2], Doron Betel[1,4], and Manuel Hidalgo[1**]

Affiliations: [1]Division of Hematology and Medical Oncology, [2]Department of Pathology, [3]Department of Surgery, [4]Computational Biology, [5]Department of Population Health Sciences, [6]Department of Radiology, Weill Cornell Medical College, New York-Presbyterian Hospital

[*]Corresponding Author
Manish A. Shah, MD, FASCO
Weill Cornell Medicine
1305 York Avenue, Y1220
New York, NY 10021
mas9313@med.cornell.edu
O: 646-962-6200
F: 646-962-1607

[**]Co-Corresponding Author
Manuel Medina Hidalgo, MD, PhD
NYU Langone Medical Oncology Associates
240 East 38th St, 20th Floor
New York, NY 10016
Manuel.hidalgo@nyulangone.org
O: 646-501-7892
F: 929-455-9660

Conflicts of Interest: This trial was developed as an investigator-initiated study and supported by Agenus Inc. Botensilimab and Balstilimab were provided by Agenus Inc. **MAS** reports research funding (institution) from MERCK, Oncolys Biopharma, Agenus, Bristol Meyers Squibb. Advisory board funding JAZZ pharmaceuticals, BeOne, and Amgen. **PMK** reports the following COIs: Scientific/Advisory Board: Eilcio, Consultancy/Advisory Board: Agenus, Astellas Pharma, Daiichi Sankyo/AstraZeneca, Bayer, Beixon Pharmaceuticals, BostonGene, Daiichi Sankyo, Delcath Systems, Eli Lilly, Eisai, Elicio Therapeutics, Exact Sciences, Foundation Medicine, Guardant, Illumina, Ipsen, Merck/MSD Oncology, Natera, Neogenomics, QED, Regeneron, RenovoRX, SAGA Diagnostics, Seagen, SIRTEX, Servier, Taiho Oncology, Tempus, and Xilio Therapeutics. Grant/Trial Support (to institution): Agenus, Merck, AAA/Novartis, Boston Scientific, Tersera. **MH** is a stock equity owner and serves as the Chairman of the Advisory Board for Nelum Pharma. **MH** also serves on the Board of Directors of Bristol Myers Squibb (BMS) and Guardant Health (GH). **MH** also declares stock and other ownership interests in Champions Oncology and InxMed, receives honoraria from Champions Oncology and Velavigo, has consulting or advisory role on OncoMatrix and InxMed, leadership roles at BMS and Guardant Health, receives funding from TopAI, Ranok Therapeutics, Incyte, and receives paid expenses from BMS and Guardant Health and royalties from Myriad for PALB2 patent. The remaining authors declare no conflicts of interest.

Article type: Research Article (Clinical Trial)
Word count: 4,911/5,000 (main text)
Tables and Figures: 6/6 (total combined)
References: 40/50
Keywords (3-8): Dual checkpoint blockade, microsatellite stable colon cancer, neoadjuvant therapy, immunotherapy, tumor microenvironment

Translational relevance (146/150 words)

Immunotherapy has limited efficacy in metastatic mismatch repair proficient (pMMR) colorectal cancer (CRC); however, when used in the neoadjuvant setting, while the primary tumor and regional lymph nodes remain intact, there is greater potential for efficacy. We present the results from the phase 2 NEST clinical trial which evaluated neoadjuvant botensilimab (BOT, Fc-enhanced anti-CTLA-4) plus balstilimab (BAL, anti-PD-1) in resectable pMMR and dMMR CRC. Treatment was feasible and associated with meaningful pathologic responses in pMMR CRC, exceeding the efficacy in metastatic pMMR CRC. Treatment-associated remodeling of the tumor immune microenvironment was observed in tumors that demonstrated a response to BOT/BAL therapy, including increased CD8+ T-cells, intratumoral FOXP3+ Treg depletion, and immune cell spatial reorganization. Responses were accompanied by circulating tumor DNA clearance and ongoing disease-free survival at follow-up. This supports further development of immunotherapy in pMMR CRC and provides clinical evidence of an anti-tumor immune response.

Abstract (250/250 words)

Purpose: Effective immunotherapy for mismatch repair proficient colorectal cancer (CRC) is lacking. We examined the safety and efficacy of the novel next-generation immune activator/Fc-enhanced CTLA-4 inhibitor botensilimab (BOT) plus PD-1 inhibitor balstilimab (BAL) in the neoadjuvant setting for patients with resectable CRC.

Patients and Methods: Patients 18 years of age or older with non-metastatic CRC awaiting surgical resection were eligible. BOT/BAL was administered followed by surgical resection. In cohort A, patients received BOT 75 mg d1 and BAL 240 mg d1, 15; in cohorts B/C, patients received 2 additional BAL doses (d29, 43). The primary study objectives were safety, feasibility (based on surgery delay), and pathologic response. Exploratory analyses examined changes in the tumor microenvironment.

Results: Twenty-four eligible patients (26 tumors, n=22 pMMR; n=4 dMMR) were enrolled (two patients had synchronous primary tumors). Neoadjuvant BOT/BAL was safe and did not delay planned surgery in any patient. The major pathologic response rate was 41% (95% CI, 21%–64%) for pMMR, and 100% (95% CI, 40%–100%) for dMMR CRC. BOT/BAL was associated with significant anti-tumor effects in the tumor microenvironment, with an increase in the density and proportion of $CD8^+$ T cells, a reduction in tumor infiltrating $FOXP3^+$ Tregs, and evidence of increased immune cell-cell interaction in responding patients.

Conclusions: These findings demonstrate safety, feasibility, and encouraging pathological responses for BOT/BAL in both non-metastatic pMMR and dMMR CRC. Tumor microenvironment remodeling suggests a robust anti-tumor immune response induced by immunotherapy. These data support the continued development of BOT/BAL in CRC.

Introduction

Colorectal cancer (CRC) is a leading cause of cancer diagnosis and cancer-related death in the United States, with approximately 154,270 new cases diagnosed and 52,900 deaths in 2025 [1]. Multidrug chemotherapy regimens in combination with targeted therapy remain the standard of care for most patients with metastatic CRC [2,3]. With the inclusion of targeted therapies and novel agents, the median overall survival for metastatic disease has improved from about 12 months to about 23 months over the past two decades [4-7]. However, there have been few advances for the treatment of locally-advanced CRC since the introduction of FOLFOX therapy in the adjuvant [8] or pre-operative (neoadjuvant) setting [9,10]. While immune checkpoint blockade has revolutionized the treatment of many solid tumors, the efficacy of traditional inhibitors of programmed cell death protein 1 (PD-1) and cytotoxic T lymphocyte-associated protein 4 (CTLA-4) in CRC has been limited to cancers that are mismatch repair deficient (dMMR)/microsatellite instability-high (MSI-H), comprising only 5%–15% of all CRC cases [11,12].

Next generation immunotherapy agents have demonstrated modest activity in mismatch repair proficient (pMMR) CRC. Botensilimab (BOT) is a second generation Fc-enhanced anti-CTLA–4 antibody that strengthens the immune synapses between antigen presenting cells and cytotoxic $CD8^+$ T cells in addition to downregulating immunosuppressive T regulatory (Treg) cells [13]. In a phase 1b trial, the combination of BOT and balstilimab (BAL), an anti-PD–1 antibody [13,14], showed an encouraging objective response rate (ORR) of 17% with a median progression free survival of 3.5 months in patients with refractory pMMR metastatic CRC [15]. A subsequent randomized phase 2 trial (NCT05608044) confirmed the efficacy of BOT/BAL in patients with refractory pMMR metastatic CRC without liver metastases, demonstrating an ORR of 19% and disease control rate of 55% [16].

Neoadjuvant immunotherapy, administered while the primary tumor and regional lymph nodes remain intact, enhances T-cell activation by leveraging abundant tumor antigens and a less developed resistance profile compared to the metastatic setting [17,18]. Neoadjuvant immunotherapy is characterized

by robust anti-tumor T cell responses potentially due to improved reactivation of tumor infiltrating PD-1^{+} cytotoxic T cells and improved priming of naïve T cells in tumor draining lymph nodes [17,19,20]. This emerging treatment paradigm has already demonstrated superior efficacy across multiple solid tumors, including melanoma [21], breast cancer [22], non-small cell lung cancer [23,24], and dMMR colorectal cancer[25-27]. In CRC, the phase 2 NICHE trial evaluated neoadjuvant combined checkpoint blockade with ipilimumab and nivolumab in patients with resectable CRC [28]. The treatment was well tolerated, and all patients underwent surgery within the predefined 6-week period. In 30 patients with non-metastatic pMMR CRC, the major pathologic response rate was 20% (n=6), including 3 patients (10%) with a complete pathologic response at the time of resection [29].

We developed the phase 2 Novel Exploratory Study to Test novel immunotherapy combinations for resectable colon cancer (NEST; NCT05571293) based on the hypothesis that dual checkpoint blockade with BOT/BAL may demonstrate improved activity in the neoadjuvant treatment of localized CRC. Herein, we present the initial findings of neoadjuvant BOT/BAL in resectable CRC. Our objectives were to examine the safety, feasibility, and preliminary efficacy of neoadjuvant therapy and to examine correlates for immune activation and pathologic response.

Methods

Study design and treatment

NEST (NCT05571293, registered in October 2022) was a single-center, non-randomized, open-label, phase 2 exploratory study, conducted at Weill Cornell Medicine/New York-Presbyterian Hospital, New York, USA. Cohort A (NEST-1) evaluated BOT 75 mg administered IV on day 1 and BAL 240 mg administered IV on days 1 and 15 (-2 to +5 days), prior to planned resection 1-6 weeks after the second BAL treatment. This initial exploratory cohort enrolled 12 patients from 3/14/2023-9/5/2023, and included 3 patients with dMMR and 9 patients with pMMR. Of the 9 pMMR patients, 2 patients were

subsequently considered inevaluable: NEST1-07 had a rectal tumor and did not undergo resection of the primary tumor, and NEST1-12 had an occult lung metastasis that was subsequently documented (**Supplementary Figure S1, Consort Diagram**).

After preliminary results from NEST-1 revealed encouraging clinical activity and safety, the study was amended (NEST-2) to include Cohort B (pMMR, 12 patients) and Cohort C (dMMR, 12 patients) and opened to enrollment on Feb 2024. Cohorts B and C evaluated BOT 75 mg administered IV on day 1 and BAL 240 mg administered IV on days 1, 15, 29, and 43 (-2 to +5 days), followed by resection 1-6 weeks following the fourth planned dose of BAL (**Supplementary Fig. S2**). Cohort B (pMMR) completed enrollment with 13 patients instead of a planned 12, due to simultaneous consent of subject 12, and Cohort C (dMMR) enrolled 1 patient. The study was closed to further enrollment at that time, as the primary focus for further development was in pMMR CRC. Patients underwent standard oncologic surgical resection combined with Enhanced Recovery After Surgery protocol [30]. All surgical-related complications were tracked for 30 days postoperatively. Following surgical resection, patients were evaluated for toxicity for up to 6 months following resection, then followed for 8 weeks by phone or with in-person evaluation for a final adverse event review.

The study was conducted in accordance with the Declaration of Helsinki and International Conference on Harmonization-Good Clinical Practice guidelines. The protocol was approved by the participating site institutional review board. All patients provided written informed consent prior to enrollment.

Patients

For all Cohorts, patients 18 years of age or older with non-metastatic histology-proven adenocarcinoma of the colon awaiting surgical resection were eligible. Patients with rectal cancer were eligible if radiotherapy was not planned and up-front resection was recommended after multidisciplinary review. Patients were required to have adequate end organ function, with an absolute neutrophil count

of ≥1.5x10^9/L, platelet count ≥100x10^9/L, hemoglobin ≥8g/dL, aspartate aminotransferase and alanine aminotransferase ≤2.5x upper limit of normal (ULN), total bilirubin ≤1.5x ULN, and calculated creatinine clearance ≥40 ml/min. Patients with metastatic cancer, those who had received prior immune checkpoint inhibitors or other systemic therapy, or with contraindications to immunotherapy (ie, history of autoimmune disease requiring steroids) were ineligible. Patients with active cardiovascular disease, such as stroke or myocardial infarction within 6 months of enrollment, unstable angina, congestive heart failure, or serious uncontrolled cardiac arrhythmia requiring medication that may prevent surgery were excluded. Pregnancy was exclusionary, and adequate birth control was required. Full eligibility criteria is provided in the protocol (**Supplementary Materials**).

Tumor mismatch repair status was assessed by immunohistochemical analysis of MLH1, MSH2, MSH6, and PMS2 proteins using biopsy samples. Loss of one or more proteins within the tumor cells indicated dMMR. Cohort A eligibility included both pMMR (n=9) and dMMR (n=3); Cohort B, pMMR (n=13); and Cohort C, dMMR (n=1).

Objectives and endpoints

The primary objectives were to assess the safety, feasibility, and efficacy (anti-tumor effects) of the BOT/BAL combination. Safety was assessed by adverse events (AEs) and serious AEs (SAEs) graded by the Common Terminology Criteria for Adverse Events (CTCAE) v5.0 up to 90 days following the last study drug dose. Any AEs/SAEs that led to a delay in surgery >6 weeks from the last treatment were recorded. Feasibility was assessed as follows: if ≥2 of the first 6 patients (or ≥4 of the full planned 12) had treatment-related surgery delays of greater than 12 weeks (Cohort A) or 16 weeks (Cohorts B or C) from treatment initiation, then the BOT/BAL combination/dosage would not be considered safe or feasible in the given population. Interim safety analyses monitored for stopping criteria, which included determination of non-feasibility, or if ≥33% of patients experienced Grade ≥3 treatment-related AEs (TRAEs).

Efficacy in Cohorts A and B was measured by pathological overall response (pOR) rate, which included pathological complete response (pCR), major pathological response (MPR), and partial response (PR). pCR was defined as no viable invasive cancer in the tumor bed or adjacent lymph nodes (tumor regression score = 0). Resected specimens with residual *in situ* disease but without an invasive component were considered pCR[26]. MPR was defined as ≥90% pathologic response (≤10% of residual viable tumor cells, tumor regression score = 1 or 2), according to the Mandard score [31]. PR was defined as ≥50–90% tumor regression. No response was defined as ≤10% tumor regression. In Cohort C, for patients who elected not to have surgery, anti-tumor effects were assessed with composite rate of clinical complete response (using clinical, radiographic, endoscopic, and/or other assessments), or MPR at 6 months. Histological evaluation of pretreatment biopsies and post-therapy resected specimens (residual tumor or tumor bed) were used to assess pathological response categories, as well as for qualitative tissue analyses.

The secondary endpoint in all Cohorts included changes in minimal residual disease by ctDNA pre- and post-surgical resection. Pathologic response in combined pMMR tumors (Cohort A pMMR, Cohort B), and dMMR tumors (Cohort A dMMR, Cohort C) was also assessed as part of a pre-specified secondary analysis. Exploratory correlative analysis included assessment of immune cells composition and biomarkers in the tumor microenvironment.

Pathological response criteria

Resected tumors were examined in their entirety, and regression of resected tumors was assessed by estimating the percentage of residual viable tumor of the macroscopically identifiable tumor bed, as identified on routine hematoxylin and eosin (H&E) staining. Regression was classified using the Mandard tumor regression grading system[31]. Major pathologic response (MPR) was defined as ≤10% of residual viable tumor cells (or ≥90% response), corresponding to Mandard tumor regression grade 1 (CR) or 2 (near-CR). Partial response (PR) was defined as at least 50% tumor regression. However, considering

the lack of consensus on the definition of PR after immunotherapy, tumors with >50% and <90% residual viable tumor would be labeled accordingly as '10%–50% tumor regression', as per the NICHE study[28]. (See **Supplementary Table S1**)

Histological evaluation

Pretreatment biopsies and post-therapy resected specimens (residual tumor or tumor bed) were histologically assessed using formalin-fixed, paraffin-embedded (FFPE) tissue sections as part of the routine clinical workflow with H&E-stained slides. Cases were centrally reviewed by an expert gastrointestinal and molecular pathologist. Histologic response was evaluated by estimation of the percentage of residual viable tumors of the macroscopically identifiable tumor bed. Tumors with prominent Crohn's-like lymphoid reaction [32], characterized by peritumoral lymphocytic aggregates found at the advancing edge of the tumor or in the tumor bed and resembling tertiary lymphoid structures (TLS), were identified. Prominence is defined as being present diffusely throughout the tumor (>50% of the tissue sampled) and containing at least 5 TLS /4x field. Select slides were also reviewed at a gastrointestinal pathology consensus conference with up to five expert gastrointestinal pathologists to help determine the percent of viable tumor cells in tumor beds.

Circulating tumor DNA assessment

Changes in circulating tumor DNA (ctDNA) were assessed using the clinical Signatera® tumor informed platform. Summary statistics including mean, standard deviation, median, and range were provided. Since this was a pilot study, the analyses are descriptive in nature, with means, medians, ranges, and/or proportions (%) where appropriate.

Immunofluorescence of the tumor microenvironment

Multiparametric *in situ* fluorescence imaging to examine the tumor microenvironment was performed using the Lunaphore COMET instrument [33,34]. A subset of pre- and post-treatment samples were examined to capture pMMR and dMMR tumors and evaluate tumors with and without responses (6 baseline biopsies and 11 resection specimens). Samples were prioritized based on availability and variability of pathologic response and MMR status. Specifically, we tried to ensure that we had at least 2 matched baseline and resection samples that had a major pathologic response and no response, as well as at least two samples with dMMR disease. Samples were stained with a multiplex immuno-oncology panel with antibodies selected from validated clones in the CLIA-certified immunohistochemistry laboratory at Weill Cornell Medicine/New York-Presbyterian Hospital (see **Figure S4A**). Panel development was performed as previously described [35]; normal human lymph node and tonsil tissues were used as controls, given adequate representation of positively-staining cells for all evaluated markers. Human tonsil tissue was included as a positive control on all study slides. Tonsil and corresponding colon FFPE blocks were sectioned at 5 µm thickness and mounted in close proximity on the same Leica charged slides. Prior to COMET processing, slides were manually dewaxed and subjected to antigen retrieval (pH 9, 20 min) using the Leica Bond RX system. To minimize tissue autofluorescence, a standard photobleaching protocol employing hydrogen peroxide and sodium hydroxide was applied. Slides were then washed with PBS and stored in solution until instrument initialization and reagent preparation were ready. Up to four slides were processed per run using the fully automated, sequential multiplex protocol based on Lunaphore's pressurized microfluidic technology. Each staining cycle comprised six steps: (1) primary antibody incubation (mouse or rabbit anti-human antibodies); (2) secondary antibody incubation with Goat Anti-Mouse Alexa Fluor Plus 555 (Thermo Scientific, Cat. A32727, 1:100) and Goat Anti-Rabbit Alexa Fluor Plus 647 (Thermo Scientific, Cat. A32733, 1:200),

followed by DAPI counterstaining (Thermo Scientific, Cat. 62248, 1:1000); (3) imaging through the DAPI, TRITC, and CY5 channels; (4) washing; (5) elution; and (6) quenching.

COMET analysis and quality control

Immunofluorescence intensity values were extracted using HALO [36]. Mean nuclear area intensity values were used for protein markers FOXP3, PCNA, PAX5, and MKI67, and mean cytoplasmic intensity values were used for the remaining markers. We defined three regions of interest (ROIs): (i) tumor in baseline biopsy sample, (ii) tumor, and (iii) tumor bed in post-treatment resection samples. After obtaining per-cell intensities for each ROI, we excluded 2% of cells with smallest size and 2% of lowest DAPI signal from further analysis to reduce artifact. We generated a binary expression matrix as described by Sanz-Moreno 2024 [33]. In brief, probe intensities within each ROI were z-score normalized and fitted onto a density function (using *gaussian_filter1d* from scipy.ndimage). The lowest peak value of the density was assumed to represent the background and to be normally distributed (*find_peaks* from scipy.signal) and cells with probe intensities above 6σ from this fitted background distribution were classified as positive for that probe.

We identified 16 cell types from a combination of 17 markers according to predefined marker scheme (see **Figure S4A**). Cells with conflicting positive markers were labeled as 'unknown'. We then focused on immune cell subtypes by excluding Vimentin, podoplanin, and SMA probes. To identify differences in cellular densities between conditions, counts of cell types were normalized to the total area of each ROI ([cell_type_count/ROI_area]*1000) and statistical differences were evaluated by the paired t-test for each cell type between different conditions.

Immune cell analyses focused on (1) differences in the tumor immune infiltrate between the baseline biopsy sample and matched resection specimens, (2) differences between responders and non-responders in the resection specimen, and (3) differences between pMMR and dMMR within the responders. We also evaluated proportions of immune cell types as a fraction of total immune cells. To

further describe the tumor immune microenvironment, cell type–combined niches were identified [37], and neighborhood enrichment analysis was performed.

Cell type–combined niches within our samples were identified following the approach by Schürch et al [37]. For each annotated cell, across all samples, we define a neighborhood region consisting of the 10 nearest neighboring cells (including the center cell) based on the Euclidean distance between spatial positions. These regions were then clustered using k-means (k=10) based on the composition of 16 cell types identified in our dataset. In addition, to focus on the immediate cellular environment of our cell types of interest, we calculated the proportion of neighboring immune cell types located within a 50-micron radius of each cell. These proportions were computed separately for each sample and then averaged across samples within each condition. To assess changes in the composition of neighboring cells between conditions, we performed statistical comparisons using the t-test.

Code availability statement

The code for correlative analyses can be found at https://github.com/abcwcm/shah_NEST2025.

Data availability statement

Data that support the findings of this study are available at https://www.ncbi.nlm.nih.gov/geo/query/acc.cgi?acc=GSE337193. Additional de-identified patient and correlative data are available based on reasonable request to the corresponding author (MAS).

Sample size and statistical methods

For Cohort A (NEST-1), enrollment was limited to no more than 25% of patients with dMMR tumors (n=3). Based on previous studies, the null hypothesis for NEST-1 was that the probability of achieving a pathologic response (eg, PR or better) to treatment is ≤5% versus the alternative H_a pathologic response rate ≥35% requires a total sample size of 12 patients (including 3 dMMR). Cohort B (NEST-2) was restricted to pMMR patients. Based on previous studies, the null hypothesis was that the

probability of achieving pOR to treatment is ≤5% versus the alternative ≥35% requires a total sample size of 12 patients with 90% power at a one-sided significance level of 0.10. Cohort C (NEST-2) was restricted to dMMR patients. The null hypothesis was that the probability of achieving pOR to treatment is ≤80% versus the alternative 100% requires a total sample size of 15 patients with 90% power at a one-sided significance level of 0.10.

Primary endpoints were summarized using counts and proportions. Safety analyses were planned for all enrolled patients and efficacy for treated patients with pathologic response assessment. Exact binomial CIs were provided for response rates. Survival probabilities were estimated by Kaplan-Meier method. Correlation between response and *KRAS/BRAF* mutational status was tested using Fisher's exact test. Correlation between response and presence of Crohn's-like reaction and tertiary lymphoid structures (TLS) was tested using Chi-squared test. Additional details are in the protocol and statistical analysis plan (**Supplementary Materials**).

Important protocol amendments

NEST-1 (Cohort A) enrolled 12 patients from 3/17/2023-9/5/2023 and demonstrated encouraging safety and feasibility results. This supported the study amendment (NEST-2), which was activated in February 2024 to enroll Cohort B (pMMR) and Cohort C (dMMR). Enrollment to the amended study (NEST-2) was from 2/14/2024 – 5/3/2024.

Results

Patients

From March 17, 2023 to May 3, 2024, 26 patients consented, and 24 were eligible for the study and received BOT/BAL (**Supplementary Fig. S1**). In NEST-1, Cohort A enrolled 10 eligible patients (n=7 pMMR, n=3 dMMR). In NEST-2, Cohort B enrolled 13 patients (all pMMR), and Cohort C enrolled one patient (dMMR). In Cohort B, two patients (NEST2-07, NEST2-08) each had synchronous primary tumors.

Therefore, the safety population included 24 patients, and 26 tumors were evaluated for efficacy. As shown in **Table 1**, the median age was 64 years (range 35–75), with an even distribution of males (n=13, 54%) and females (n=11, 46%). Half of the study population was White, and the majority (n=21, 88%) were non-Hispanic. Fourteen patients (58%) had radiologically locally advanced tumors (T3+) and 42% (n=10) had radiographically discernable lymph nodes. The representativeness of the study population is shown in **Supplementary Table S2**.

At the data cutoff of March 31, 2026, the median follow-up duration was 32.2 and 23.5 months, respectively, for Cohort A and Cohorts B/C. The study was closed after the completion of enrollment to Cohort B and one patient enrolled in Cohort C, due to an administrative reason (PMK left the institution).

Safety and feasibility

Neoadjuvant BOT/BAL was safe with no delays to planned surgery in any patient. Median time to surgery from start of treatment was 29 days (range 21–37) for Cohort A, and 55 days (range 21–104) for Cohorts B and C. All patients underwent minimal invasive resection (laparoscopic or robotic), with one conversion to open surgery. Among all Cohorts, median hospitalization length of stay was 2 days (range 1–14).

TRAEs are provided in **Supplementary Table S3**. No Grade 4 toxicities occurred. In Cohort A, one patient had Grade 2 diarrhea/colitis that resolved with TNF-alpha inhibition (eg. infliximab). We also observed five patients with a common symptom pattern of fever, chills, and fatigue, noted within 2 weeks of BOT/BAL administration. These symptoms were readily managed by proactive supportive care, which included non-steroidal anti-inflammatory medication (eg, naproxen) or acetaminophen as an anti-pyretic, and rarely, a short course of steroids. Four out of five patients with these symptoms were able to receive their second dose of BAL without delay; the fifth patient had fevers accompanied by Grade 3 fatigue. In total, 2 out of 10 patients in Cohort A required high dose steroids, and 1 patient required TNFα inhibition.

In Cohorts B and C, five patients had immune-mediated toxicity: colitis/diarrhea (n=5; grade 2 (n=2), grade 3 (n=3)), grade 2 myositis/myocarditis (n=1) requiring the use of high dose steroids and TNFα inhibitor (infliximab) therapy (**Supplementary Table S3**). Of the 14 patients enrolled in Cohorts B and C, 9 received all planned treatment (BOT/BAL on day 1 followed by 3 doses of BAL), 3 patients received 3 BAL doses (treatment held due to colitis (n=3)), and 2 patients received 2 BAL doses (treatment held for colitis (n=1) and myositis (n=1)). Among all 24 patients (all Cohorts), 2 patients (8%) had a Clavien-Dindo Classification Grade I complication. No deaths or study discontinuations were observed.

Efficacy: pathologic response

The pOR rate in Cohort A was 70% (n=7/10 patients) overall, and 57% (n=4/7) for pMMR patients. In Cohort B, the pOR rate was 62% (n=8/13; all pMMR). **Fig. 1A** shows a representative example of clinical response following treatment in a pMMR/MSS patient.

The pathologic response for each tumor is shown in **Fig. 1B**. In Cohort A, 2/7 (29%; 95% CI 4%–71%) pMMR tumors demonstrated MPR, and in Cohort B, the MPR rate was 7/15 (47%; 95% CI 21%–73%) pMMR tumors. In a pre-specified secondary analysis, we examined all pMMR tumors from Cohorts A and B combined (n=22 tumors). For all pMMR tumors, the pathologic response rate (>50% tumoral response) was 59% (13/22; 95% CI, 36%–79%), the MPR rate was 41% (9/22; 95% CI, 21%–64%), and the pCR rate was 32% (7/22; 95% CI 14%–55%). Molecular annotation was available in all 22 pMMR tumors (**Supplementary Table S4**). Although there were no associations between tumor mutation burden or PD-L1 combined positive score with treatment response, tumors with *KRAS* G12D (n=2) or an activating *BRAF* mutation (n=1, *BRAF* V600R) had no pathologic response (0%–10% response). In contrast, only 3/19 tumors (14%) with other *KRAS/BRAF* mutations (n=2/7), or that were *KRAS* and *BRAF* wild type (n=1/12), had no pathologic response (p=0.048; **Supplementary Table S5**).

For dMMR tumors (n=4 overall), the MPR rate was 100% (95% CI, 40%–100%). Two had pCR, and one each showed 99% and 98% treatment effect (each having 1–3 small clusters of cancer cells identified within mucin pools).

As of the data cutoff, no patients had CRC recurrence, as shown in the progression free survival Kaplan Meier curve (**Fig. 1C**). ctDNA was examined in 15 patients using the commercial tumor informed Signatera assay. Nine had ctDNA collected at baseline (prior to study initiation) and all were positive (range 0.06–54.65 MTM/ml). Of these patients, we collected a pre-surgical sample (within 30 days of surgery) in 8 patients, and 7 patients (88%) had clearance of their ctDNA (**Supplementary Table S6**). As shown in **Fig. 1D**, ctDNA remained undetectable following resection in all patients.

Histological analysis of tumor response

Qualitative review of baseline H&E-stained tissue showed no discernible histologic differences in the immune infiltrate between responding and nonresponding tumors. However, the post-treatment tumor bed in cases achieving MPR demonstrated several distinctive histological features. These tumor beds were characterized by dense mixed inflammatory infiltrates, composed largely of lymphocytes, plasma cells, and histiocytes, accompanied by mucosal-based granulation tissue with neovascularization, acellular mucin pools, and submucosal fibrosis. Eosinophils and neutrophils were also variably present (**Supplementary Fig. S3**).

As expected, three of four dMMR tumors exhibited prominent Crohn's-like reaction surrounding the tumor bed indicative of a robust anti-tumor immune response. However, this reaction was also present in 73% of pMMR cases with >50% pathologic response after treatment, compared to only 13% without pathologic response, revealing a significant association between the development of prominent Crohn's-like reaction and MPR following BOT/BAL (p=0.028, **Supplementary Table S7**). In all dMMR and pMMR tumors with MPR, large acellular mucin pools were striking, with a subset containing sparse clusters of residual tumor cells. In pMMR tumors with PR (50%–90% pathologic regression),

inflammatory infiltrates were dense and qualitatively similar to those observed in MPR cases but were most prominent at the tumor-stromal interface (periphery of viable tumor) and deep within the wall of the colon. In cases with a PR, the tumor bed had residual viable tumor that tended to be superficially oriented within the center of the tumor bed, a pattern distinctive from the haphazard arrangement typically seen following neoadjuvant chemotherapy. These residual tumors had viable tumor glands that frequently showed evidence of ongoing immune-mediated destruction with disrupted crypts, incomplete lumens, and frequent luminal microabscesses with necrosis.

Analysis of the tumor immune microenvironment

Using the multiplex imaging COMET platform, we studied the composition and spatial organization of the tumor immune microenvironment. We identified 286,935 total immune cells within the regions of interest (tumor, peritumoral area, tumor bed) across all samples (**Supplementary Fig. S4A, S4B**). Our analysis revealed notable differences in the character and organization of the immune infiltrate between responding and non-responding tumors at the time of resection. Tumors achieving MPR tended to demonstrate a robust, organized immune infiltrate with co-localization of multiple cell types, a pattern consistent with coordinated anti-tumor immunity (**Figs. 2A, 2B**). In contrast, tumors with minimal to no pathologic response exhibited spatially isolated immune infiltrates with a greater proportion of $FOXP3^+$ regulatory T cells (Tregs) (**Figs. 2C, 2D**). We quantified these differences across defined regions of interest to characterize how BOT/BAL immunotherapy modulates the tumor immune microenvironment in both responding and non-responding tumors, and to identify potential differences between pMMR and dMMR responses.

Analysis of baseline biopsies and matched tumor resection specimens suggests treatment-induced remodeling of the tumor-immune landscape. Following BOT/BAL, we observed a numerical decrease in the density of both $CD3^+FOXP3^+$ and $CD3^+CD4^+FOXP3^+$ Tregs, concurrent with a 13-fold increase in CD8+ T cell density (**Fig. 3A**). This shift in the density of infiltrating immune cell subsets from

baseline to resection was also accompanied by changes in the proportion of immune cell populations at the time of resection, with $CD8^+$ T cells increasing from 5% of the immune infiltrate at baseline to 30% in the resection specimen (p=0.077, **Supplementary Fig. S5A**). This resulted in a 21-fold increase in the CD8+/Treg ratio from baseline (CD8+/Treg 0.286) to resection (CD8+/Treg 6.20), consistent with an activated anti-tumor immune response (**Supplementary Fig. S5B**). These changes in the immune infiltration were similar when limiting the analysis to pMMR CRC (**Supplement Figures S11-S14**).

Notably, we observed an increased immune infiltrate in the resection specimens of responders as compared with non-responders (**Fig. 3B**). The infiltrating immune cell density in non-responding tumors was 0.52 immune cells/μm, whereas in responding tumors it was 3.1 immune cells/μm (p=0.0048), largely due to changes in the density and proportion of effector cells. Specifically, CD8+ T cell density was 19-fold higher in responding versus non-responding tumors (p=0.022), while B cell density was 59-fold higher (p=0.07). These differences in immune cell density were associated with compositional shifts in effector immune cells. Specifically, $CD8^+$ T cells and B cells each comprised 34% of the immune infiltrate in responding tumors, compared to 15% and 6%, respectively, in non-responding tumors (p=0.11 for CD8+ T cells and p=0.018 for B cells, **Supplementary Fig. S5C**). While the density of Tregs is paradoxically higher in responding tumors (p=0.039), they comprise a smaller portion of the total immune infiltrate in responding tumors compared to non-responding tumors (15% vs 31%, respectively). This would indicate that there is proportionally an even greater increase in the infiltration of CD8+ T cells in responding tumors. The net result is a notable difference in $CD8^+$ T cell/Treg ratio (0.52 in non-response, 5.27 in response; **Supplementary Fig. S5D**), consistent with activation of an anti-tumor immune response in tumors that have pathological evidence of response following BOT/BAL.

We observed no significant difference in the immune cell infiltrate in the baseline biopsy samples of responders versus non-responders (**Supplementary Fig. S6**), possibly suggesting that pre-

existing inflammation was not a major driver of BOT/BAL response. However, analysis of matched baseline and resection specimens confirmed that the CD8+ T cell/Treg ratio improved in both responders and non-responders following BOT/BAL therapy (**Supplementary Fig. S7**), but numerically, to a greater extent in responders (**Fig. 4**).

This difference in the immune cell composition in responders versus non-responders was accompanied by notable differences in the spatial distances between immune cells (**Supplementary Fig. S8**). Specifically, $CD8^+$ T cells and B cells were significantly closer to plasma cells in responders versus non-responders, whereas Tregs were further away from CD4+ T cells in responders versus non-responders. These differences in distances between key regulatory and effector immune cells suggest potential differences in local immune cell microenvironments in tumors that demonstrated a response to BOT/BAL versus non-response. The differences in distances between key immune cell mediators between responders and non-responders were similar in pMMR tumors, suggesting a similar immune microenvironment in responders, independent of MMR status **(Supplement Fig S14).**

Cellular neighborhood enrichment analysis confirmed spatial reorganization of the immune microenvironment following BOT/BAL. We identified 10 distinct cellular neighborhoods, or niches, defined by the spatial proximity of different cell types within 50 mm radius in pathological regions of interest (**Supplementary Fig. S9A**). Responding tumors were characterized by immune-enriched communities, particularly niche 3 (B cell-enriched) and niche 6 (CD8+ T cell-enriched), which were almost exclusively observed in responders, consistent with the TLSs observed histologically (**Supplementary Fig. S9B**). In contrast, non-responding tumors were enriched by niches 0, 4, and 8, characterized by epithelial cells, stroma, and an immune cluster with elevated macrophages (M1 and M2) and CD4+ Tregs, respectively. Quantitative analysis of the local cellular environment of $CD8^+$ T cells, Tregs, and B cells, further illustrated this spatial reorganization (**Fig. 5**).

At baseline, these key immune cells were primarily surrounded by stromal cells, tumor epithelium, and lymphatic endothelium across all patients. Following therapy, this pattern persisted in non-responding tumors, where immune cells remained isolated within stromal and epithelial compartments. However, in responding tumor beds, the majority of cells within the niche surrounding CD8+ T cells, Tregs, and B cells were other immune cells creating the organized, immune-dense microenvironment (**Figs. 5 and 2**).

While both dMMR and pMMR tumors demonstrated robust immune infiltration following BOT/BAL in responding cases, we observed quantitative differences in immune composition in these two CRC subtypes (**Supplementary Fig. S10A**). dMMR tumors exhibited a numerically higher proportion of CD8+ T cells (51% vs 27% in pMMR responders, p=0.13), consistent with the inherently more immunogenic nature of dMMR tumors. Despite this difference, both dMMR and pMMR responders showed prominent B cell and plasma cell enrichment in their local microenvironment (**Supplementary Fig. S10B**), suggesting that organized humoral immunity contributes to therapeutic response across these molecular subtypes.

Discussion

Neoadjuvant immunotherapy for solid tumor malignancies is an emerging paradigm based on strong scientific rationale[17,19] and has demonstrated compelling efficacy across several malignancies[21-24] (reviewed by Awada, et al.[38]). In CRC, most of the available data is in patients with dMMR. For example, neoadjuvant immunotherapy has been established in patients with dMMR rectal cancer with a remarkable pathologic and clinical response rate and excellent overall survival[39]. For dMMR colon cancer, immunotherapy is also now established as the standard of care for adjuvant therapy for locally advanced disease[40], and emerging evidence strongly supports its use in the neoadjuvant setting as

well[41]. However, the data for the use of neoadjuvant immunotherapy for pMMR colon cancer is limited[29].

Here, we report the initial safety and efficacy of BOT/BAL as a novel, next-generation, dual checkpoint inhibition combination for locoregional colon cancer. In patients with dMMR CRC, this combination achieved a major pathologic response in 4/4 cases, consistent with the known activity of checkpoint blockade in dMMR CRC. However, in patients with pMMR CRC, we observed a major pathologic response rate of 41% (n=9/22), including 32% (n=7/22) of patients whose tumors achieved a pCR. We also noted that 7/8 patients who were ctDNA positive at baseline had evidence of ctDNA clearance prior to resection, further supporting the activation of anti-tumor immunity with this novel checkpoint combination.

The phase 2 NICHE-1 trial initially examined the dual checkpoint combination of nivolumab and ipilimumab in a cohort of 31 patients with pMMR colon cancer, with half of the patients randomly assigned to also receive celecoxib [28,29]. Similar to the NICHE-1 experience, in both NEST cohorts (NEST-1 and NEST-2), neoadjuvant BOT/BAL was safe and tolerable, with no patient experiencing a delay in proceeding to surgery. In NICHE-1, the median time from study initiation to surgery was 33 days, similar to our experience in NEST-1 (29 days). In NICHE-1, in a similarly staged population of pMMR colon cancer (eg, 51% locally advanced), nivolumab/ipilimumab demonstrated modest anti-tumor activity, with an MPR of 19% (n=6/31) [29]. In NEST, with the combination of BOT/BAL, the MPR was 41%, with 32% of patients experiencing a pCR. Both NEST and NICHE studies demonstrate remarkable activity of dual checkpoint blockade in the neoadjuvant treatment setting for pMMR CRC. In our study, with 24-33 months of follow up, our disease-free survival (DFS) rate is 100%. In NICHE-2, with longer follow up, the 3-year DFS rate is 93% [42]. Alternatively, with neoadjuvant chemotherapy in the FOXTROT study, the recurrence rate at 2 years was 16.9% [10].

The MPR rate in NEST-2 is numerically higher (47%) as compared with NEST-1 (27%). We note the study was not designed to compare the two treatment schedules. More patients experienced immune-mediated AEs in NEST-2 (n=5/14 vs 2/10 in NEST-1), and 5/14 patients did not receive the fourth scheduled BAL dose. Although this toxicity suggests that more than two doses of immunotherapy in the neoadjuvant setting may not be feasible, it is also not clear, if there is indeed a greater pathologic response with NEST-2, whether it is because of the additional BAL doses or the increased time to surgery, which would allow for more time for the immune system to attack the tumor.

Our initial correlative analysis of NEST reveals notable changes in the immune density, composition, and immune cell niche from baseline to resection in responding tumors. We identified depletion of the Treg population in the resected specimen when compared with the matching baseline biopsy in all tumors, but more profound Treg depletion in tumors that responded to BOT/BAL. This is consistent with the mechanism of action of BOT [13], indicating activation of anti-tumor immunity, and is similar to NICHE-1 where there was evidence of immune activation in both responding and non-responding cases. However, in tumors that achieved a major pathologic response, we observed co-localization of immune cells, in particular $CD8^+$ T cells and B cells, supporting the concept of the development of an organized anti-tumor immune response and immune activation in response to BOT/BAL. Alternatively, in non-responding tumors, although we did see evidence of Treg depletion, and an increase in $CD8^+$ T cells, we found no evidence that they co-localized or were organized to generate an anti-tumor immune response. Further, although there was a numerically greater infiltration of CD8+ T cells in dMMR tumors compared with pMMR tumors with major pathologic response, resulting in a larger $CD8^+$ T cell/ Treg ratio, we found similar patterns of immune cell microenvironments, suggesting similar immune activation with BOT/BAL therapy in both dMMR and pMMR tumors.

Our observation that activating mutations of the RAS/RAF pathway may be associated with less activity with BOT/BAL is limited by the small samples size. In non-small cell lung cancer, *KRAS* G12D is

associated with resistance to immunotherapy, and an isogenic lung cancer model showed that *KRAS* G12D is associated with specific reduction in $CD8^+$ T cell infiltration and reduced PD-L1 expression [43]. *KRAS* G12D mutations are associated with significant reduction in IFN-a and IFN-g signaling in CRC and reduced T cell infiltrate [44], both of which would predict resistance to immunotherapy, consistent with our observations. Alternatively, in dMMR metastatic colorectal cancer, BRAF V600E mutation does not predict resistance to immunotherapy in a large retrospective analysis[45]. These preliminary data will need further evaluation and validation.

This study has several limitations. The sample size of both NEST-1 and NEST-2 is small, and the follow-up period of the study is also relatively short; thus, the durable efficacy of the combination of BOT/BAL is unknown. Further, the study was underpowered to determine the optimal duration of neoadjuvant therapy versus the number of immunotherapy treatments prior to surgical resection. However, this data highlights critical knowledge gaps in advancing checkpoint blockade for neoadjuvant CRC treatment, including: (1) does therapy duration affect local and systemic outcomes, (2) are there biomarkers predictive of resistance, and fundamentally, (3) why is immune activation effective in the localized setting but diminished once metastases develop?

Despite these limitations, the NEST study provides preliminary evidence of the efficacy and safety of BOT/BAL in the neoadjuvant treatment setting. The compelling pathologic response, coupled with the DFS and evidence of ctDNA clearance prior to resection with BOT/BAL therapy, as well as the reorganization of the local immune infiltrate suggesting activation of a robust anti-tumor immune response, suggest the continued development of BOT/BAL in the neoadjuvant treatment setting for pMMR CRC.

Authors' Disclosures

MAS reports research funding (institution) from MERCK, Oncolsys Biopharma, Agenus, Bristol Meyers Squibb. Advisory board funding JAZZ pharmaceuticals, BeOne, and Amgen. **PMK** reports the following COIs: Scientific/Advisory Board: Eilcio, Consultancy/Advisory Board: Agenus, Astellas Pharma, Daiichi Sankyo/AstraZeneca, Bayer, Beixon Pharmaceuticals, BostonGene, Daiichi Sankyo, Delcath Systems, Eli Lilly, Eisai, Elicio Therapeutics, Exact Sciences, Foundation Medicine, Guardant, Illumina, Ipsen, Merck/MSD Oncology, Natera, Neogenomics, QED, Regeneron, RenovoRX, SAGA Diagnostics, Seagen, SIRTEX, Servier, Taiho Oncology, Tempus, and Xilio Therapeutics. Grant/Trial Support (to institution): Agenus, Merck, AAA/Novartis, Boston Scientific, Tersera. **MH** is a stock equity owner and serves as the Chairman of the Advisory Board for Nelum Pharma. **MH** also serves on the Board of Directors of Bristol Myers Squibb (BMS) and Guardant Health (GH). **MH** also declares stock and other ownership interests in Champions Oncology and InxMed, receives honoraria from Champions Oncology and Velavigo, has consulting or advisory role on OncoMatrix and InxMed, leadership roles at BMS and Guardant Health, receives funding from TopAI, Ranok Therapeutics, Incyte, and receives paid expenses from BMS and Guardant Health and royalties from Myriad for PALB2 patent.

Authors' Contributions

We followed ICGME rules for authorship. MAS, MH, PMK, EH, MDJ, DB, and SP each made substantial contributions to study design, acquisition, analysis, and interpretation of the clinical and correlative data. MA, SK, CO, ZC, HY, FS, SS, AN, DS, AO, KG, LL, AP, and PG each contributed to acquisition of the data. MAS, EH, MDJ, and MH drafted the manuscript critically for important intellectual content. All authors provided final approval of the manuscript and are accountable for all aspects of the work and its integrity.

Acknowledgements

We would like to thank all participating patients for their efforts and commitment to advance treatment options in colorectal cancer. This trial was developed as an investigator initiated study and was supported by Agenus Inc. Botensilimab and Balstilimab were provided by Agenus Inc. Agenus Inc had no role in the study design, data analysis, or interpretation of results. Independent editorial/medical writing support was provided by Elizabeth G. Wheatley, PhD, CMPP (MidCoast Medical Writing, LLC; funded by Agenus Inc. without intellectual influence).

References

1. Siegel, R.L., Kratzer, T.B., Giaquinto, A.N., Sung, H. & Jemal, A. Cancer Statistics, 2025. *CA Cancer J Clin* **75**, 10-45. (2025).
2. Biller, L.H. & Schrag, D. Diagnosis and Treatment of Metastatic Colorectal Cancer: A Review. *JAMA* **325**, 669-685. (2021).
3. Ciardiello, F*., et al.* Clinical Management of metastatic colorectal cancer in the era of precision medicine. *CA Cancer J Clin* **72**, 372-401. (2022).
4. Jawed, I., Wilkerson, J., Prasad, V., Duffy, A.G. & Fojo, T. Colorectal Cancer Survival Gains and Novel Treatment regimens: a systematic review and analysis. *JAMA Oncol* **1**, 787-795. (2015).
5. Morris, V.K*., et al.* Treatment of metastatic colorectal cancer: ASCO Guideline. *J Clin Oncol* **41**, 678-700. (2023).
6. Shen, C*., et al.* Overall Survival in phase 3 clinical trials and the surveillance, epidemiology, and end results database in pateints with metastatic colorectal cancer: 1986-2016: a systematic review. *JAMA Netw Open* **5**, e2213588. (2022).
7. Elez, E*., et al.* Encorafenib, cetuximab, and mFOLFOX6 in BRAF-mutated colorectal cancer. *N Engl J Med* **392**, 2425-2437. (2025).
8. Andre, T*., et al.* Oxaliplatin, fluorouracil, and leucovorin as adjuvant treatment for colon cancer. *N Engl J Med* **350**, 2343-2351 (2004).
9. Hu, H*., et al.* Neoadjuvant chemotherapy with oxaliplatin and fluoropyrimidine versus upfront surgery for localy advanced colon cancer: the randomized, phase III OPTICAL Trial. *J Clin Oncol* **42**, 2978-2988 (2024).
10. Morton, D*., et al.* Preoperative chemotherapy for operatble colon cancer: Mature results of an international randomized controlled trial. *J Clin Oncol* **41**, 1541-1552 (2023).
11. Andre, T*., et al.* Pembrolizumab in Microsatellite-Instability-High Advanced Colorectal Cancer. *N Engl J Med* **383**, 2207-2218 (2020).
12. Franke, A.J*., et al.* Immunotherapy for Colorectal Cancer: A Review of Current and Novel Therapeutic Approaches. *J Natl Cancer Inst* **111**, 1131-1141 (2019).
13. Chand, D*., et al.* Botensilimab, an Fc-enhanced anti-CTLA-4 Antibody, is effective against tumors poorly responsibe to conventional immunotherapy. *Cancer discovery* **14**, 2407-2429. (2024).
14. O'Malley, D.M*., et al.* Phase II study of the safety and efficacy of the anti-PD-1 antibody balstilimab in patients with recurrent and/or metastatic cervical cancer. *Gynecol Oncol* **163**, 274-280. (2021).
15. Bullock, A.J*., et al.* Botensilimab plus balstilimab in relapsed/refractory microsatellite stable metastatic colorectal cancer: a phase 1 trial. *Nat Med* **30**, 2558-2567 (2024).
16. Fakih, M., Segal, N.H., Schlechter, B.L., Andre, T. & al., e. Preliminary results from a randomized, open-label, phase 2 study of botensilimab (BOT) with or without balstilimab (BAL) in refractor microsatellite stable metastatic colorectal cancer with no liver metastases (MSS mCRC NLM). *J Clin Oncol* **43**, abs 23 (2025).
17. Topalian, S.L., Taube, J.M. & Pardoll, D.M. Neoadjuvant checkpoint blockade for cancer immunotherapy. *Science* **367**, eaax0182 (2020).
18. Wei, S.C., Duffy, C.R. & Allison, J.P. Fundamental mechanisms of immune checkpoint blockade therapy. *Cancer discovery* **8**, 1069-1086. (2018).
19. Liu, J*., et al.* Improved efficacy of neoadjuvant compared to adjuvant immunotherapy to eradiate metastatic diseae. *Cancer discovery* **6**, 1382-1399. (2018).
20. O'Donnell, J.S., Hoefsmit, E.P., Smyth, M.J., Blank, C.U. & Teng, M.W.L. The promise of neoadjuvant immunotherapy and surgery for cancer treatment. *Clin Cancer Res* **25**, 5743-5751. (2019).

21. Blank, C.U*., et al.* Neoadjuvant nivolumab and ipilimumab in resectable stage III melanoma. *N Engl J Med* **391**, 1696-1708. (2024).
22. Schmid, P*., et al.* Event-free survival with pembrolizumab in early triple-negative breast cancer. *N Engl J Med* **386**, 556-567. (2022).
23. Forde, P.M*., et al.* Neoadjuvant PD-1 blockade in resectable lung cancer. *N Engl J Med* **378**, 1976-1986. (2018).
24. Ricciuti, B*., et al.* Neoadjuvant PD-1 and PD-L! blockade with chemotherapy for borderline resectable and unresectable stage III non-small cell lung cancer. . *JAMA Oncol* **11**, 735-741. (2025).
25. de Gooyer, P.G.M*., et al.* Neoadjuvant nivolumab and relatlimab in locally advanced MMR-deficient colon cancer: a phase 2 trial. . *Nat Med* **30**, 3284-3290. (2024).
26. Wang, F*., et al.* Neoadjuvant treatment of IBI310 plus sintilimab in locally advanced MSI-H/dMMR colon cancer: a randomized phase 1b study. *Cancer Cell* **43**, 1958-1967. (2025).
27. Cercek, A*., et al.* PD-1 blockade in mismatch repair-deficient, locally advanced rectal cancer. . *N Engl J Med* **386**, 2363-2376. (2022).
28. Chalabi, M*., et al.* Neoadjuvant immunotherapy leads to pathological responses in MMR-proficient and MMR-deficient early-stage colon cancers. *Nat Med* **26**, 566-576 (2020).
29. Tan, P.B*., et al.* Neoadjuvant immunotherapy in mismatch-repair-proficient colon cancers. *Nature* **[epub ahead of print]**(2025).
30. Sauro, K.M*., et al.* Enhanced recovery after surgery guidelines and hospital length of stay, readmission, complicaitons, and mortality: A meta-analysis of randomized clinical trials. *JAMA Netw Open* **7**, e2417310. (2024).
31. Mandard, A.M*., et al.* Pathologic assessment of tumor regression after preoperative chemoradiotherapy of esophageal carcinoma. Clinicopathologic correlations. *Cancer* **73**, 2680-2686 (1994).
32. Maoz, A., Dennis, M. & Greenson, J.K. The Crohn's-Like lymphoid reaction to colorectal cancer-Tertiary lymphoid structures with immunoloic and potentially therapeutic relevance in colorectal cancer. . *Front Immunol* **10**, 1884. (2019).
33. Navikas, V*., et al.* Semi-automated approaches for interrogating spacial heterogeneity of tissue samples. *Sci Rep* **14**, 5025. (2024).
34. Rivest, F*., et al.* Fully automated sequential immunofluorescence (seqIF) for hyperplex spatial proteomics. *Sci Rep* **13**, 16994. (2023).
35. Rivest, F*., et al.* Fully automated sequential immunofluorescence (seqIF) for hyperplex spatial proteomics. *Sci Rep* **13**, 16994 (2023).
36. Horai, Y*., et al.* Quantification of histopathological findings using a novel image analysis platform. *J. Toxicol Pathol* **32**, 319-327. (2019).
37. Schurch, C.M*., et al.* Coordinated cellular neighborhoods orchestrate antitumoral immunity at the colorectal cancer invasive front. *Cell* **182**, 1341-1359.e1319 (2020).
38. Awada, G*., et al.* The rapidly evolving paradigm of neoadjuvant immunotherapy across cancer types. *Nat Cancer* **6**, 967-987. (2025).
39. Cercek, A*., et al.* PD-1 Blockade in Mismatch repair-deficient, locally advanced rectal cancer. *N Engl J Med* **386**, 2363-2376 (2022).
40. Sinicrope, F.A*., et al.* Randomized trial of standard chemotherapy alone or combined with atezolizumab as adjuvant therapy for patients with stage III deficient DNA mismatch repair (dMMR) colon cancer (Alliance A021502; ATOMIC). *J Clin Oncol* **43**, abs LBA1 (2025).
41. Chalabi, M*., et al.* Neoadjuvant immunotherapy in locally advanced mismatch repair-deficient colon cancer. *N Engl J Med* **390**, 1949-1958. (2024).

42. Tan, P.B.*, et al.* Neoadjuvant immunotherapy in mismatch-repair-proficient colon cancers. *Nature* **648**, 726-735. (2025).
43. Liu, C.*, et al.* KRAS-G12D mutation drives immune suppression and the primary resistance of anti-PD-1/PD-L1 immunotherapy in non-small cell lung cancer. *Cancer Commun* **42**, 828-847. (2022).
44. Brubaker, D.K.*, et al.* Proteogenomic network analysis of context-specific KRAS signaling in mouse-to-human cross-species translation. *Cell Systemis* **9**, 258-270. (2019).
45. Gallois, C.*, et al.* Prognostic impact of the BRAF V600E mutation in patients with MSI-high metastatic colorectal cancer treated with immune checkpoint inhibitors. *Eur J Cancer* **227**(2025).

FIGURE LEGENDS

Figure 1. Efficacy of neoadjuvant BOT/BAL in patients with localized colon cancer. (**A**) Patient with clinical response. (**B**) Pathologic tumor response for all n=26 tumors, shown as Cohort A/NEST-1 pMMR (n=7), Cohort B/NEST-2 pMMR (n=15), and dMMR (n=3 Cohort A, n=1 Cohort C). (**C**) Kaplan Meier curve for disease free survival for Cohort A (NEST-1) and Cohorts B/C (NEST-2). (**D**) Clinical circulating tumor DNA for patients (n=15) pre- and following initiation of therapy.

Figure 2. Multiplex immunofluorescent images of a tumor bed in a responding patient (**A** low power, **B** high power), and the tumor of a non-responding patient (**C** low power, **D** high power). Pathologic response is associated with a dense and diverse immune infiltrate, consistent with activation of anti-tumor immunity following BOT/BAL.

Figure 3. Density of immune infiltrate (**A**) in matched baseline versus resection paired specimens, and in the (**B**) resection specimens of responders and non-responders. (**A**) The density of Tregs is numerically reduced in the resection specimen compared with baseline, whereas CD8_T cell density is increased. (**B**) The density of immune cells in responders is significantly higher than of non-responders (3.1 cells/μm v 0.52 cells/μm, p=0.0048), dominated by an infiltrate of B cells and CD8+ T cells. Pathologic treatment effect (0-100%) is indicated.

Figure 4. Composition of the immune infiltrate from baseline to resection, in both responding and non-responding tumors. The proportion of Tregs decreased following BOT/BAL therapy, whereas CD8+ T cells increased. This results in a numerical increase in the CD8+/Treg T cell ratio, more in the responders versus the non-responders. The log rank p-value is provided comparing the CD8+T cell/ Treg ratio in each condition.

Figure 5. The immune cell community is distinct in responding (n=7) versus non-responding (n=4) tumors. The pie chart identifies the prevalence of cells within 50 microns of the cell type of interest. At baseline, the microenvironment of immune cells of interest (CD8+ T cells, Tregs, and B cells) is predominantly composed of lymphatic endothelium, stromal cells, and undefined T cells. Conversely, these immune cells are notably infrequently found co-localizing with other B-cells, CD4+ T-cells, or CD8+ T-cells. In non-responding patients, the microenvironment of the immune cells of interest is largely composed of stromal and smooth muscle cells, accompanied by a notable increase in M2 macrophages. We also observe that the local microenvironment of plasma cells is mostly comprised of M2 macrophages. In contrast, responding patients are characterized by a markedly different immune cell microenvironment composition, with relative enrichment for B cells, T cells (CD4+, CD8+ and other undefined subtypes), and Tregs (accounting for >50% of cells within these localized regions).

Table 1. Patient demographics.

	Total (N=24)	Cohort A (n=10)	Cohort B (n=13)	Cohort C (n=1)	dMMR/MSI-H (n=4)
Age, Median (Q1, Q3)	64 (46, 73)	57 (35, 69)	68 (59, 75)	71	61 (43, 72)
Male:Female	13:11	5:5	8:6	1 male	3:1
Race					
White	12	5	6	1	3
Asian	4	1	3	0	0
Black	4	2	2	0	0
Other	4	2	2	0	1
Ethnicity					
Hispanic	1	1	0	0	0
Non-Hispanic	21	9	11	1	4
Other	2	0	2	0	0
Tumor Location					
Left sided	14	5	9	0	3
Right sided	12	5	6	1	1
Clinical T Stage					
T1/T2	10	1	9	1	1
T3+	14	9	4	0	3
Clinical N Stage					
N+	10	9	1	0	3
Nx (or N0)	16	1	14	1	1

Figure 1

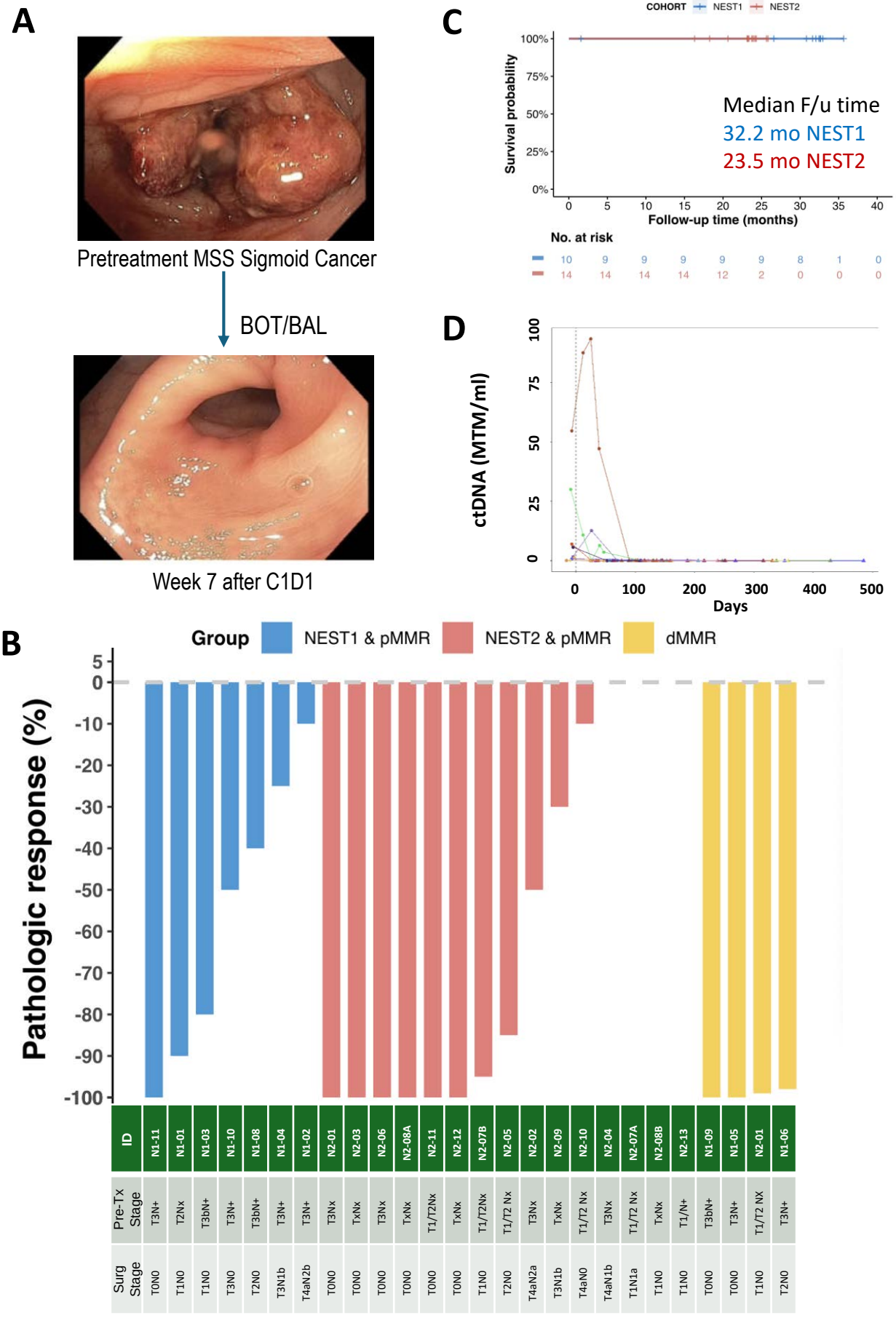

Figure 2.

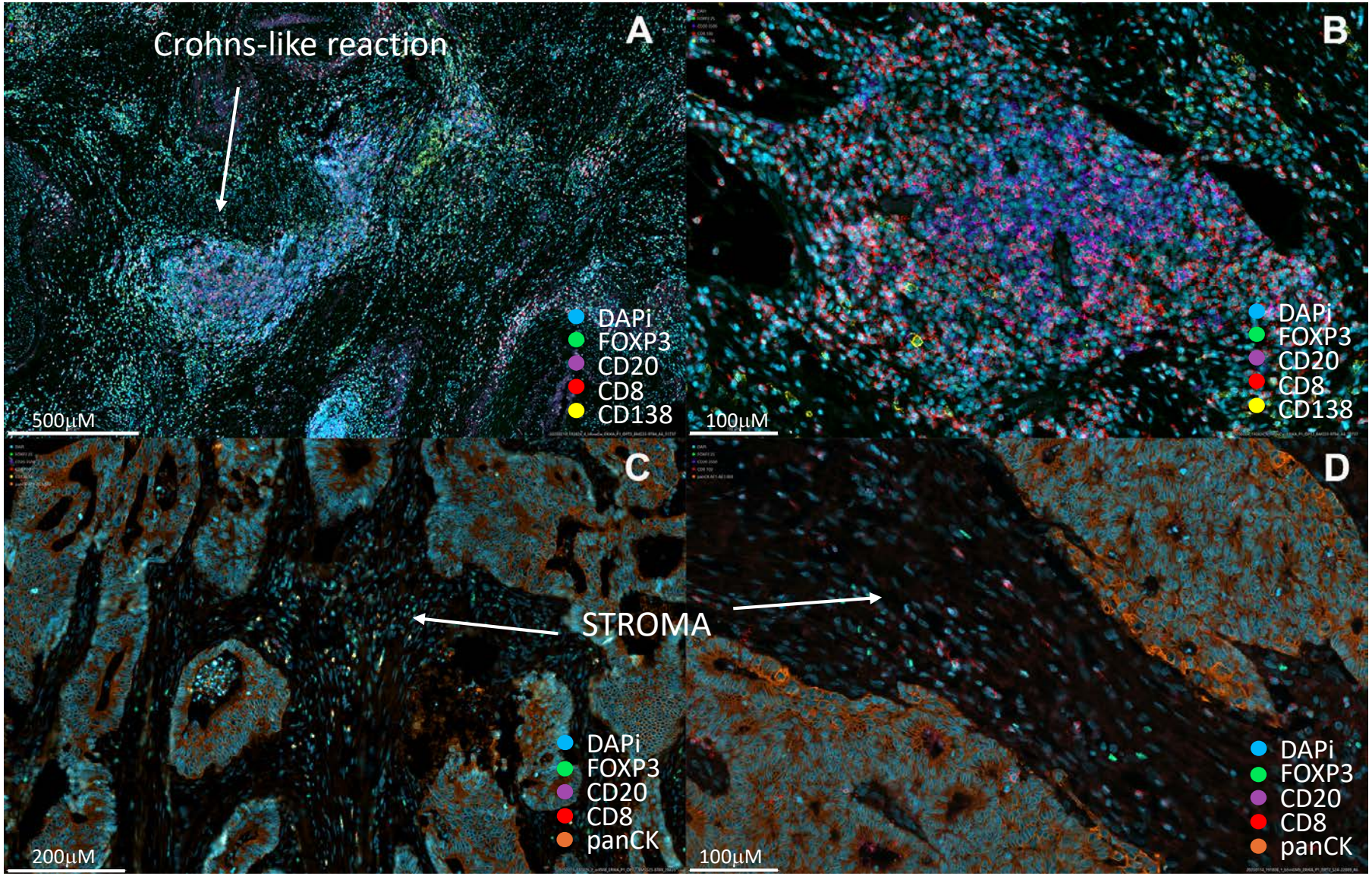

Figure 3

A

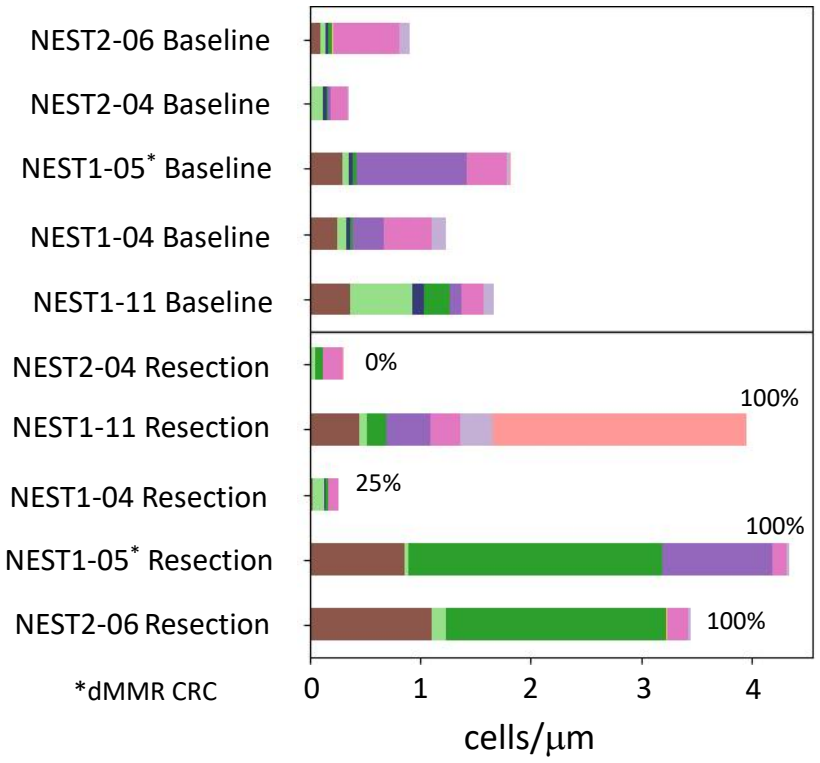

Immune cell type	Baseline Density	Resection Density	p-value
Treg (FOXP3⁺)	0.35	0.17	p=0.1
CD4_Treg (CD4⁺FOXP3⁺)	0.045	0.003	p=0.05
CD4_T cell	0.18	0.075	p=0.34
CD8_Treg (CD8⁺FOXP3⁺)	0.002	0.003	p=0.75
CD8_T cell	0.069	0.91	p=0.1
B cell	0.20	0.49	p=0.2

B

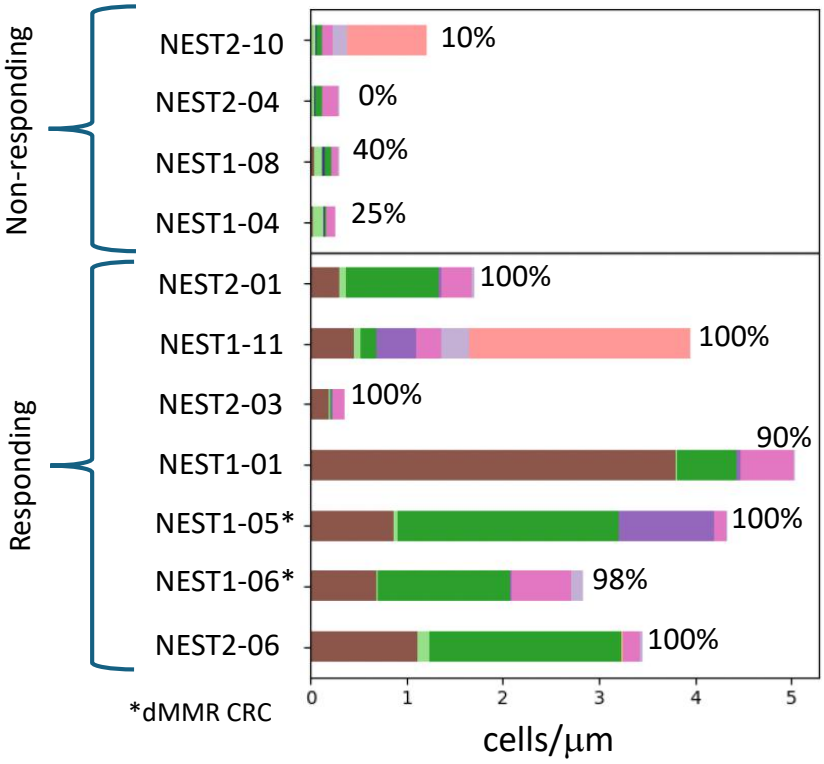

Immune cell type	Responder	Non-Responder	p-value
Treg (FOXP3⁺)	0.31	0.11	p=0.036
CD4_Treg (CD4⁺FOXP3⁺)	0.0005	0.013	p=0.093
CD4_T cell	0.047	0.070	p=0.38
CD8_Treg (CD8⁺FOXP3⁺)	0.002	0.0005	p=0.38
CD8_T cell	1.07	0.05	p=0.022
B cell	1.06	0.02	p=0.070

Figure 4.

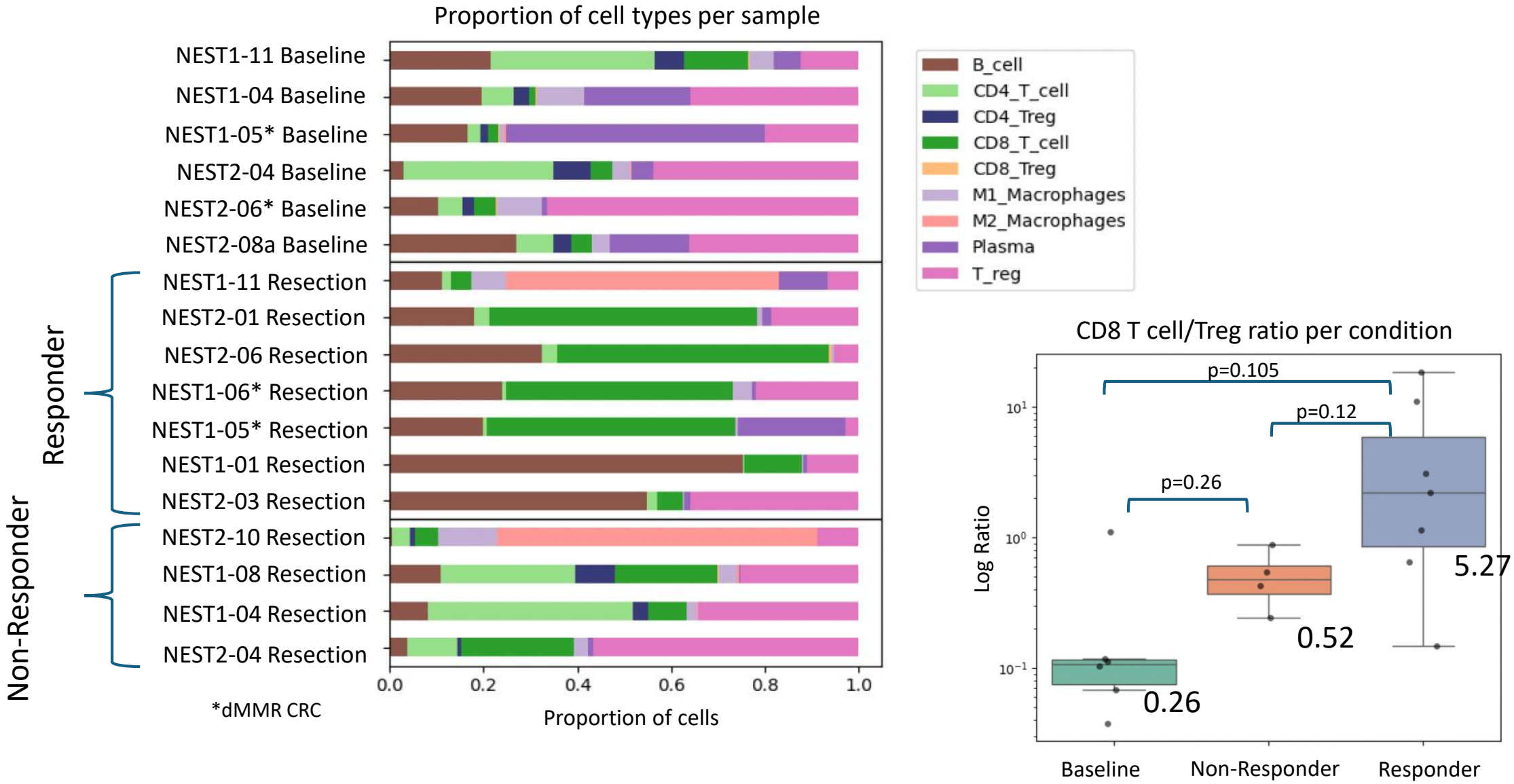

Figure 5. CD8 T cell Targets